Journal of Alloys and Compounds 851 (2021) 156912

Contents lists available at ScienceDirect

Journal of Alloys and Compounds

journal homepage: http://www.elsevier.com/locate/jalcom

# The influence of metallic Bi in $BiVO_4$ semiconductor for artificial photosynthesis

Juliana F. de Brito [a, 1], Patricia G. Corradini [a, 1], Maria Valnice B. Zanoni [b], Frank Marken [c], Lucia H. Mascaro [a, *]

[a] Department of Chemistry, Federal University of São Carlos, Rod. Washington Luiz, Km 235, CEP 13565-905, São Carlos-SP, Brazil
[b] Institute of Chemistry - Araraquara, UNESP, Rua Francisco Degni, 55, Bairro Quitandinha, 14800-900, Araraquara, SP, Brazil
[c] Department of Chemistry, University of Bath, Claverton Down, Bath, BA2 7AY, UK

ARTICLE INFO

*Article history:*
Received 16 June 2020
Received in revised form
24 August 2020
Accepted 26 August 2020
Available online 28 August 2020

*Keywords:*
Metallic bismuth
Lamellar $BiVO_4$
Photocatalysis
Reduction of $CO_2$
Methanol production

ABSTRACT

$BiVO_4$ is a non-titania inorganic photocatalyst recognized as an effective visible-light-driven semiconductor that has been shown to be effective for $CO_2$ reduction. However, some characteristics, such as a low separation rate of photogenerated electron-hole pairs and low mobility of electron-hole carriers, are still challenges to the widespread use of this semiconductor. In this paper, the influence of metallic Bi on the $CO_2$ photoreduction activity was evaluated for the $BiVO_4$ semiconductor. Bi–$BiVO_4$ catalysts were prepared by microwave heating at 240 °C, employing different reaction times and magnetic stirring regimes. Metallic Bi improved the catalytic activity of $BiVO_4$ for $CO_2$ reduction, enhancing the absorption of visible light and promoting internal photoemission of electrons in the metal-semiconductor interface, which improves the electron density in the surface of the catalyst. This resulted in an astonishing concentration of methanol; Bi–$BiVO_4$ prepared at 240 °C, for 5 min, and without magnetic stirring, produces around 5.0 mmol $L^{-1}$ $g^{-1}_{catalyst}$ of methanol and 40 μmol $L^{-1}$ $g^{-1}_{catalyst}$ of acetone after 240 min of reaction. The mechanism of charge transfer between the $BiVO_4$ and the metallic Bi is influenced by the size of the microsphere crystallites, moreover, the production of methanol increased as the Bi grain size decreased.



## 1. Introduction

The photocatalysis technique has been applied in the conversion of photon energy into chemical energy for the photosynthetic reduction of $CO_2$, mainly using simple and practical powder-based photocatalysts [1–3]. Among several options of powder-based photocatalysts, $BiVO_4$ is a non-titania inorganic catalyst recognized as an effective visible-light-driven semiconductor [4–6]. This catalyst attracted considerable attention in the last decade due to its non-toxic nature, high stability, low cost, and a visible-light response with a band gap of 2.4 eV [7,8]. Due to those characteristics, $BiVO_4$ semiconductors are effective in many different applications, such as $O_2$ production from water splitting [9–11], degradation of organic compounds [12,13], and $CO_2$ reduction [5,14–16].

Although widely applied, $BiVO_4$ suffers from deactivation with time [16], low separation rate of photogenerated electron-hole pairs [17], low mobility of electron-hole carriers, and poor charge migration [18,19]. Those characteristics impact the efficiency and result in reduced reaction yields. The rate of generation of the electron-hole pair, its lifetime, dissociation, and recombination provide some of the key factors for an efficient semiconductor photocatalyst [20]. An alternative to improve the photoactivity of $BiVO_4$ is to modify the catalyst with metal species or with heterojunctions.

The combination of metals and semiconductors can create intermediate energy levels inside the band gap of the semiconductor, favoring the transport of the photogenerated electrons to the conduction band (CB) [21]. For this purpose, three strategies to modify the semiconductor with metals are commonly used, all of which reduce the binding energy of the valence electrons: (*i*) substitution of an anion by a less electronegative species, such as N or S, to obtain *p* states with lower binding energy; (*ii*) addition of

* Corresponding author.
*E-mail address:* lmascaro@pq.cnpq.br (L.H. Mascaro).
[1] These authors contributed equally to the manuscript and should be considered first coauthors.

https://doi.org/10.1016/j.jallcom.2020.156912
0925-8388/

cations with occupied *d* states (e.g., Cu or Ag); and (*iii*) addition of cations with occupied *s* states (e.g., Bi or Sn) [22].

Some reports in the literature described efforts to improve the catalytic activity of several photocatalysts introducing heterojunctions [23–29], which is also applicable to $BiVO_4$ photocatalysts, especially by chemical modifications. Kim and co-workers [30] developed a $BiVO_4$/C/$Cu_2O$ photocatalyst for the photocatalytic reduction of $CO_2$ with formation of CO. The combination of both semiconductors, $BiVO_4$ and $Cu_2O$, resulted in a significant improvement in the charge separation and light-harvesting properties. Chen and co-workers [17] synthesized Cu/$BiVO_4$ photocatalysts with visible-light response by microwave-assisted hydrothermal methods. The presence of Cu increased the absorption of visible light by the semiconductor and induced a redshift in the absorption band. Gromboni et al. [31] modified nanostructured $BiVO_4$ with a coating of microporous $Al_2O_3$ using a sol-gel method; this modification led to a reduction in the pseudo-capacitance and improved quantum efficiency. Wang et al. [32] developed AgI/$BiVO_4$ composites and observed that an appropriate wettability is essential to improve the photocatalytic activity. Merupo et al. [18] doped a $BiVO_4$ powder with molybdenum (Mo) through a sol-gel method, which promoted a slight change in the band gap, thereby enhancing the rate of light absorption. Corradini et al. [5] prepared a $BiVO_4$–$Bi_2O_3$ powdered catalyst through a microwave-based technique, which improved the $BiVO_4$ charge transfer for $CO_2$ reduction, promoting the synthesis of methanol and acetone.

In the present paper, the $CO_2$ photoreduction activity of $BiVO_4$ was improved by the addition of a cocatalyst: metallic Bi. Bi–$BiVO_4$ materials were prepared by a rapid microwave synthesis technique, employing different reaction times, and stirring regimes. The as-synthesized semiconductors were applied in the $CO_2$ reduction in aqueous medium using standard photocatalysis techniques with photosynthetic fuel generation. Although the Bi–$BiVO_4$ promoted the same products as those reported using $BiVO_4$, an improvement in the photoexcited charge transfer mechanism was observed.

## 2. Materials and methods

### 2.1. Synthesis of Bi-based materials

The catalysts were prepared using a methodology adapted from Gao et al. [33] and Corradini et al. [5]. The precursor was a solution of 1.7 mmol $BiCl_3$ (Sigma-Aldrich®, 98%) and 0.35 g of cetyl trimethyl ammonium bromide (CTAB, Sigma-Aldrich®, 98%) in 20 mL of ethylene glycol, followed by addition of 2.3 mmol $Na_3VO_4$ (Sigma-Aldrich®, 90%) under magnetic stirring. The solution was submitted to a microwave system (Anton-Paar®), at 240 °C for 5 or 15 min, under magnetic stirring at 0 or 1200 rpm in the course of the microwave irradiation. After the system was cooled to room temperature, the catalysts were centrifuged with ethanol and water, filtered, and dried at 50 °C for 12 h.

### 2.2. Physical characterization

The Bi–$BiVO_4$ catalysts were characterized by X-ray diffraction (XRD), Raman spectroscopy, scanning electron microscopy (SEM), transmission electron microscopy (TEM), energy-dispersive X-ray spectroscopy (EDS), and UV–Vis Diffuse Reflectance Spectroscopy (DRS). The XRD diffractograms were obtained on a Siemens AXS Analyticas X-Ray D 5005 diffractometer with scans between 10° and 80° at 2° $min^{-1}$. SEM images were obtained using a microscope FEI, model Inspect F50; while X-ray scatter spectra were also determined on an SEM FEI, model Inspect EBSD. Raman measurements were performed on a Micro Raman Horiba iHR 550 spectrophotometer with a 633 nm laser. Absorption spectra were obtained on a Varian Model Cary 5G UV–vis–NIR spectrophotometer coupled with an integrating sphere with a wavelength range from 250 to 800 nm. The analysis of the DRS spectra was performed by traditional methods, employing the Kubelka-Munk function and Tauc equation [34], to relate the energy of the incident photons and the band gap ($E_g$) of the material. TEM analyses were performed with a TECNAI G2F20 microscope with the dispersed samples deposited on carbon-coated copper grids. EDS analyses were performed with Zeiss equipment, model 35.

### 2.3. Photocatalytic reduction of $CO_2$

The $CO_2$ photoreduction experiments were described in our previous study [5]. Briefly, 0.3 g of the catalyst was suspended in 220 mL of $NaHCO_3$ (0.1 mol $L^{-1}$, pH 8.0). The photoreduction proceeded in an internal illumination reactor, controlling the temperature at 5 °C. The mixture was magnetically stirred in the dark for 30 min before irradiation, to allow the system to reach an adsorption/desorption equilibrium. The commercial Hg lamp employed in the system was a Philips 125 W lamp, model HPL-N 1542, with UV–Vis irradiation. At determined time intervals, 2.0 mL suspensions were collected and analyzed using gas chromatography with flame ionization detection (GC-FID).

## 3. Results and discussion

### 3.1. Physical characterization of Bi–$BiVO_4$ catalysts

Fig. 1a presents the XRD patterns for all Bi–$BiVO_4$ catalysts prepared using the microwave synthesis technique at 240 °C employing different synthesis times and magnetic stirring regimes. All samples presented the same diffraction peaks, which can be indexed to the rhombohedral structure [space group: *R3m* (166)] of elemental Bi (JCPDS no 85-1329 - Fig. 1a inset) [35,36]. The prominent peak at 27.1° refers to the plane Bi (012). There was no difference in the plane intensity ratio between the samples and the card reference, indicating that the structure is polycrystalline [37]. The presence of $BiVO_4$ could not be confirmed by XRD, probably because of the low crystallinity of lamellar $BiVO_4$ structures, a morphology commonly obtained from the employed synthesis route [5,33]. However, analyzing the Raman spectra (Fig. 1b), it is possible to identify bands at 817, 367, and 203 $cm^{-1}$, which indicate the vibrations of monoclinic $BiVO_4$ [7,9]. The high-intensity band at 817 $cm^{-1}$ is attributed to the symmetric and asymmetric stretching of V–O bonds [38], while the band at 203 $cm^{-1}$ is related to the external mode of the $VO_4^{3-}$ tetrahedron [39]. The peaks around 510 $cm^{-1}$ correspond to the Si substrate. Those results imply that the as-synthetized materials are a composition of metallic Bi and monoclinic $BiVO_4$.

The atomic ratio of Bi to $BiVO_4$ was estimated by EDS and is shown in Table 1. For the synthesis without agitation, the ratio was close to 1, while the agitation promoted a reduction of this percentage. Agitation makes it difficult to form germination points for crystal growth, which could result in a decreased Bi/$BiVO_4$ ratio [40]. To observe the effect of agitation on the sizes of the Bi crystals, the crystallite sizes were calculated for all as-prepared samples using the XRD peak widths for peaks with greater intensity, relative to the plane [012] ($2\theta = 27.1°$, Fig. 1a), and the Scherrer equation (eq. (1)):

$$D_{Sch} = K\lambda / \beta_{hkl}\cos(\theta) \quad (1)$$

Here, $D_{Sch}$ is the crystallite size, K is a constant equal to 0.9 for the spherical morphology, λ is the XRD incidence wavelength of Cu-k$\alpha$ radiation (0.154 nm), $\beta_{hkl}$ is the half-width of the peak and $\theta$ is

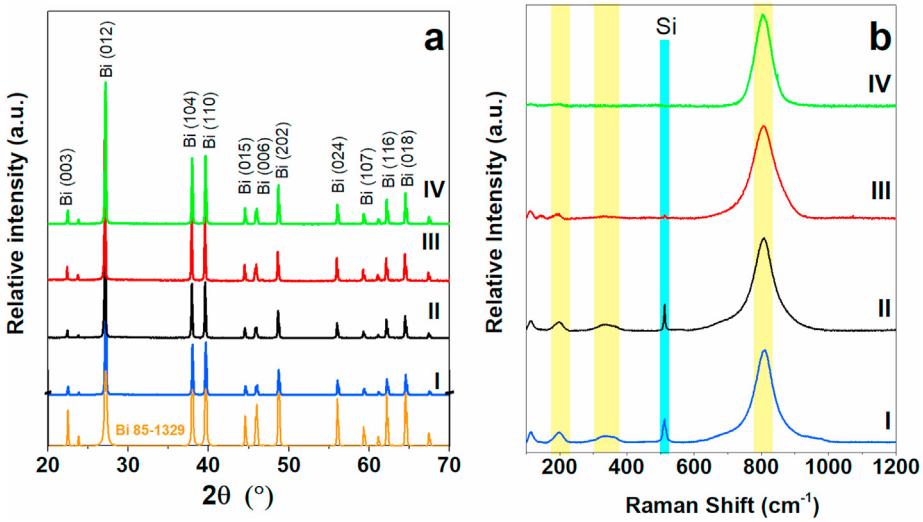


**Fig. 1.** a) XRD and b) Raman of the Bi−$BiVO_4$ semiconductor prepared by microwave synthesis at 240 °C and (I) 5 min without magnetic stirring, (II) 15 min without magnetic stirring, (III) 5 min under magnetic stirring at 1200 rpm, and (IV) 15 min under magnetic stirring at 1200 rpm.

**Table 1**
The atomic proportion of Bi/$BiVO_4$ estimated by EDS, average crystallite lattice size for the (012) plane of metallic Bi, and band gap values obtained for the different Bi−$BiVO_4$ catalysts.

| Samples | Time (min) | Magnetic Stirring velocity (rpm) | Bi/$BiVO_4$ ratio | Average crystallite lattice size (nm) | Band gap value (eV) |
|---|---|---|---|---|---|
| I | 5 | 0 | 1.1 | 52.7 | 3.0 |
| II | 15 | 0 | 1.0 | 53.5 | 2.9 |
| III | 5 | 1200 | 0.8 | 56.5 | 3.0 |
| IV | 15 | 1200 | 0.6 | 55.7 | 2.9 |

the (hkl) peak position [41,42]. The average crystallite size for metallic Bi is presented in Table 1; the results show that both synthesis time and magnetic stirring can affect the size of the metallic Bi crystallites. However, the magnetic stirring variable presents a more intense effect than the time for the crystalline lattice. The stirring effect can cause changes in nucleation and growth processes, especially due to the presence of Taylor vortices or turbulent flow in the solution [43]. The increase in temperature makes the stirring effect even more significant for the growth of crystal seeds inserted in the flowing solution, since the onset of crystallization under extreme temperatures is only possible with a significant flow [44]. In the present study, using the condition of 1200 rpm, it is possible to obtain a slightly larger crystal size, compared to the crystals obtained without agitation.

SEM images for Bi−$BiVO_4$ are presented in Fig. 2. For all as-synthetized samples, it is possible to observe a mixture of smooth and rough microspheres with different sizes. The literature reports that, for microwave synthesis, the temperature drastically influences the morphology for $BiVO_4$ semiconductors, resulting in lamellar forms of $BiVO_4$ at 160 °C [5,33]. Ke et al. [10] also reported a significant temperature effect on the morphology via the hydrothermal route. The authors observed the formation of $BiVO_4$ microspheres at 160 °C and lamellar $BiVO_4$ at 200 °C. According to Wu et al. [39], the $Bi^{3+}/V^{5+}$ molar ratio is the main factor that defines the morphology. The authors obtained smooth microspheres reaching the molar ratio of 0.56; however, lower $Bi^{3+}/V^{5+}$ molar ratios, such as 0.50, were already able to change the material into a cake-like morphology. The molar ratios for the catalysts analyzed in this study were calculated by TEM and are discussed below.

Transmission electron microscopy (TEM) images are shown in Fig. 3 for different magnifications and different regions for the Bi−$BiVO_4$ semiconductor powder prepared using microwave synthesis at 240 °C for 5 min without magnetic stirring (sample I). TEM images of the other as-prepared catalyst samples were very similar. Through TEM, it is possible to observe that the powdered catalyst is composed of microspheres with different sizes and that there is a lamellar form close to the microspheres. This distribution is observed for all samples. It is known that the lamellar form is related to the $BiVO_4$ semiconductor, based on other reports from the literature [5,10,33]. Therefore, the microspheres are probably metallic Bi.

To confirm the composition of each morphology, Fig. 4 presents the TEM image and the localized EDS data obtained for the Bi−$BiVO_4$ semiconductor prepared using the microwave synthesis technique at 240 °C for 5 min without magnetic stirring. Fig. 4a highlights two different regions labeled as 1 and 2, which are represented in Fig. 4b and c, respectively. The presence of bismuth (Bi) was confirmed in the microspheres, but vanadium (V) or oxygen (O) were not detected in the microspheres, indicating that the microspheres observed in the SEM and TEM images are related to metallic Bi. On the other hand, Fig. 4c presents all three components of the material, Bi, V, and O, indicating that the lamellar form is related to the $BiVO_4$ semiconductor. The $Bi^{3+}/V^{5+}$ molar ratio obtained from Fig. 4c is of 0.75, drastically different from the value of 0.56 expected for $BiVO_4$ microspheres [39]. Furthermore, the temperature induces the formation of lamellar $BiVO_4$, corroborating the idea that the microspheres are composed of only metallic Bi. The presence of copper (Cu) in both EDS is related to the copper grid used in the analysis.

The absorption of light in the UV−Vis region was evaluated by DRS analysis for the Bi−$BiVO_4$ catalysts. Fig. 5a shows the absorbance spectra for Bi−$BiVO_4$ prepared at 240 °C, 15 min, and 1200 rpm as an example compared to the pure $BiVO_4$ prepared by the microwave method at 140 °C for 10 min [5]. Generally, the wide

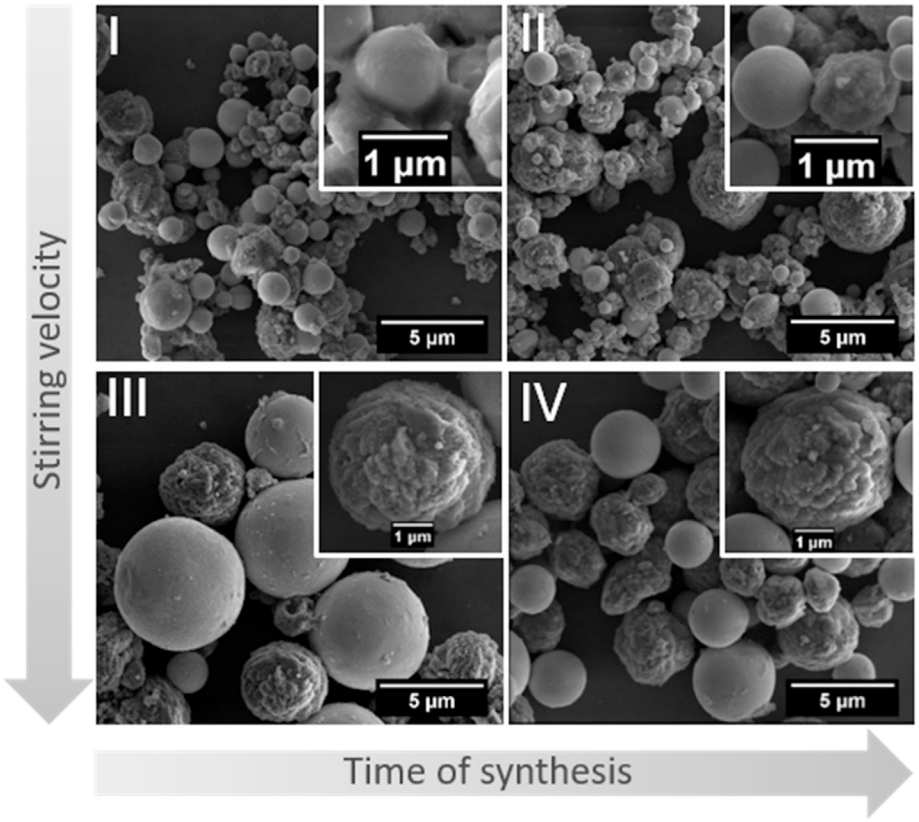


**Fig. 2.** SEM images of Bi–$BiVO_4$ catalysts obtained by microwave synthesis at 240 °C and (I) 5 min without magnetic stirring, (II) 15 min without magnetic stirring, (III) 5 min under magnetic stirring at 1200 rpm, and (IV) 15 min under magnetic stirring at 1200 rpm.

optical absorption of all different materials in this study was very similar. The catalysts presented a greater response in the UV region, although there is also a significant absorption in the visible part of the spectrum up to 800 nm. Comparing the Bi–$BiVO_4$ absorbance with the result for the pure $BiVO_4$ semiconductor, it is possible to observe that, despite a higher absorbance value in the analyzed region for Bi–$BiVO_4$, both systems have similar profiles that are also similar to the ones reported in the literature for $BiVO_4$ [10,15,33].

In Fig. 5b, the Tauc plot is represented to illustrate the determination of the band gap for the Bi–$BiVO_4$ catalyst, compared to the band gap of the pure $BiVO_4$ catalyst. A value of 2.90 eV was obtained for the band gap of Bi–$BiVO_4$through extrapolation of the direct permissible electronic transition curve. Almost the same value was obtained for all of the prepared catalyst materials, as seen in Table 1. The band gap calculated by the same method for the pure $BiVO_4$, also prepared by microwave synthesis, was of 3.05 eV. Normally, the band gap reported for the monoclinic $BiVO_4$ semiconductor is around 2.4 eV [10,16]. However, wider ranges of band gap energies have been reported in the literature for similar materials [8]. According to Walsh et al. [22], the inclusion of cations, which reduce the binding energy of valence electrons for occupied *s* states ($ns^2$), such as $Bi^{3+}$, should raise the valence band level and consequently reduce the band gap of the metal oxides. Thus, Bi insertion may have caused a slight reduction of the $BiVO_4$ band gap.

### 3.2. Reduction of $CO_2$ using Bi–$BiVO_4$ catalysts

The characterized catalysts were evaluated regarding the photosynthetic $CO_2$ reduction under aqueous conditions using the photocatalysis technique in a cooling system. The product fuels obtained throughout 240 min of photoreaction using Bi–$BiVO_4$ as semiconductors are presented in Fig. 6. It was possible to quantify methanol (Fig. 6a) and acetone (Fig. 6b) as products generated from the $CO_2$ reduction for all catalysts studied. Other alcohols, aldehydes, and organic acids were investigated but not detected within the confidence limit of quantification (0.2 µmol $L^{-1}$).

The highest rate of formation for both products (methanol and acetone) was obtained with the semiconductor prepared at 240 °C, 5 min, and without magnetic stirring. In the case of methanol production, this catalyst was able to generate around 5.0 mmol $L^{-1}$ $g^{-1}_{catalyst}$ after 120 min of photocatalysis, while the other catalysts did not reach a production greater than 1.0 mmol $L^{-1}$ $g^{-1}_{catalyst}$ for methanol. For acetone production, the Bi–$BiVO_4$ prepared at 240 °C, 5 min and without magnetic stirring, reached 40 µmol $L^{-1}$ $g^{-1}_{catalyst}$ after 240 min of reaction, while the catalyst prepared with a synthesis time of 15 min and magnetic stirring of 1200 rpm was able to generate around 20 µmol $L^{-1}$ $g^{-1}_{catalyst}$ of acetone during the same reaction time. The other catalysts maintained the production around 5.0 µmol $L^{-1}$ $g^{-1}_{catalyst}$ of acetone after 240 min. In our previous study [5], we reported the formation of methanol and acetone by photocatalytic reduction of $CO_2$ using $BiVO_4$ synthesized through a microwave route. A high methanol production was obtained with $BiVO_4$ prepared at 160 °C, reaching 1.50 mmol $L^{-1}$ $g^{-1}_{catalyst}$ of methanol after 120 min of reaction. However, this is three times less than the methanol production obtained with the Bi–$BiVO_4$ catalyst. In both cases, the formation of acetone reached similar values, with an increase around 30% in the concentration of acetone after the insertion of metallic Bi.

It is easily observed that methanol was not appreciably formed during the first 60 min of $CO_2$ reduction and that it is only after 120 min that it was possible to quantify this product. The first and main step in the photosynthesis of this product is the reaction

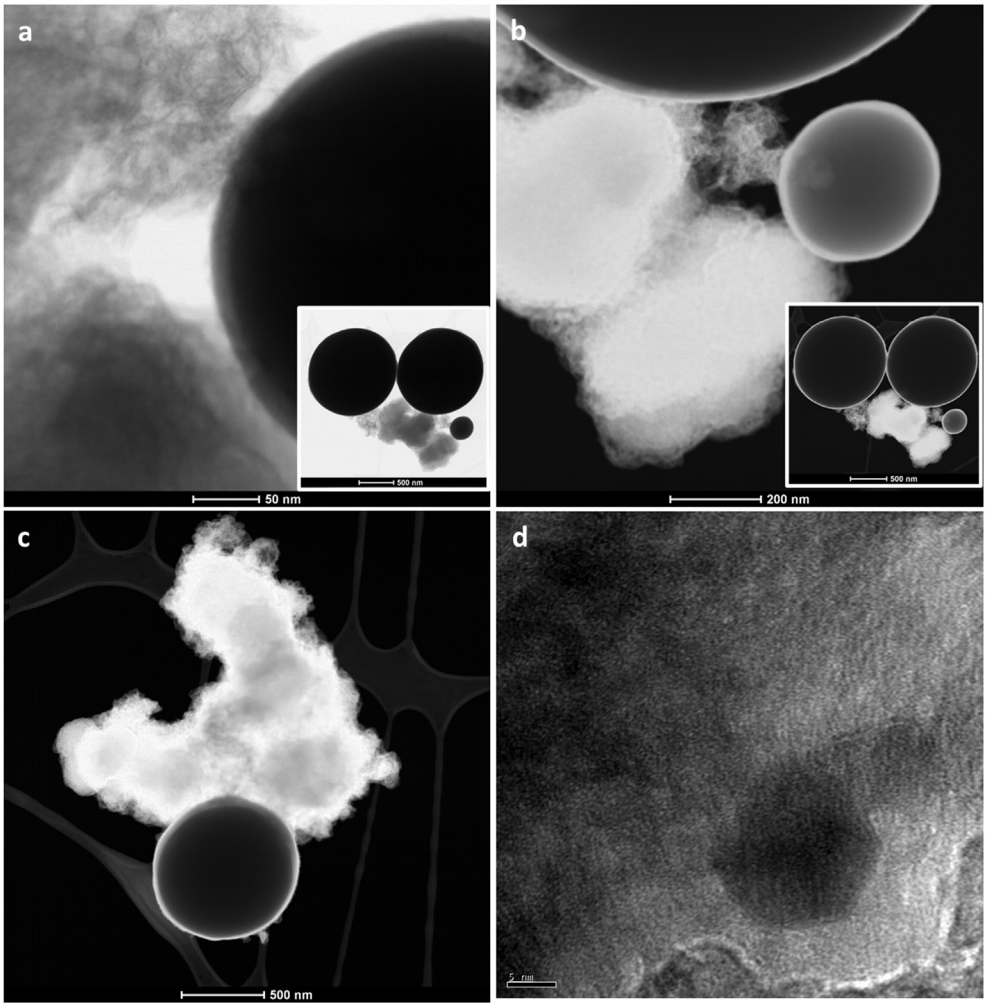


**Fig. 3.** TEM images from different regions of the Bi–$BiVO_4$ semiconductor prepared using microwave synthesis at 240 °C for 5 min without magnetic stirring (sample I).

between the $CO_2$ and the photogenerated $e^-$ at the surface of the catalyst, forming the intermediate $^{\bullet}CO_2^-$ [45,46]. This is the rate-limiting step owing to the large reorganizational energy that exists between the radical $^{\bullet}CO_2^-$ formed and the original linear $CO_2$ molecule [47]. The following steps involve reactions of protons and electrons with $^{\bullet}CO_2^-$ and, at this point, there is a high kinetic dependence on the concentration of protons available in the supporting electrolyte and on the electron density in the semiconductor surface [48]. The time necessary to identify the formation of the first products probably is related to these intermediate stages of the reaction. The formation and accumulation of $^{\bullet}CO_2^-$ and other radicals must be required for the formation of methanol and other products. As soon as a minimum concentration is reached, the reaction probably becomes auto-catalytic and the reaction kinetics changes dramatically [49].

The formation of acetone by photocatalysis with $BiVO_4$ was reported for the first time in our previous study [5]. The present modification of the $BiVO_4$ surface with metallic Bi did not change the products obtained from the $CO_2$ reduction, since methanol and acetone were the only quantified products in both cases. However, the methanol production increased threefold by the addition of Bi in the $BiVO_4$ powdered catalyst compared to pure $BiVO_4$ [5]. Similar quantities of methanol have been obtained only through bias potential assistance [45,50,51] and through different methods that do not use light as the only energy source.

Comparing those previous results with the present study, it is possible to observe the influence of metallic Bi on the catalytic activity for $CO_2$ reduction. For the samples studied herein, the catalyst with the most expressive formation of products from $CO_2$ reduction has the smallest average crystallite lattice size for metallic Bi (012) (Table 1) and highest Bi/$BiVO_4$ ratio, which leads to a possible conclusion that the mechanism of charge transfer between the $BiVO_4$ and the metallic Bi is influenced by the size of the microsphere crystallites. The architecture of the catalyst can improve the results for photosynthetic $CO_2$ reduction, due to the surface area and velocity of charge carrier transport, which are prerequisites for an attractive semiconductor regarding this subject [52]. In this case, the smaller crystallite sizes for metallic Bi may provide greater surface area and charge carrier transportation, contributing to a more effective reduction of $CO_2$.

In the literature, the improvement due to the presence of the metal is explained by the formation of a Schottky barrier at the metal-semiconductor interface, leading to a reduced recombination rate between the photogenerated electrons and holes, which improves the photosynthetic activity of the material [53–55]. Bismuth has an interesting behavior since it can also be photo-excited. In this Bi–$BiVO_4$ catalyst, metallic Bi is the key to enhance the photocatalytic capabilities of the $BiVO_4$ semiconductor. According to Castillo and Peter [56], metallic Bi can generate internal photoemission of electrons, which improves the electron density in the

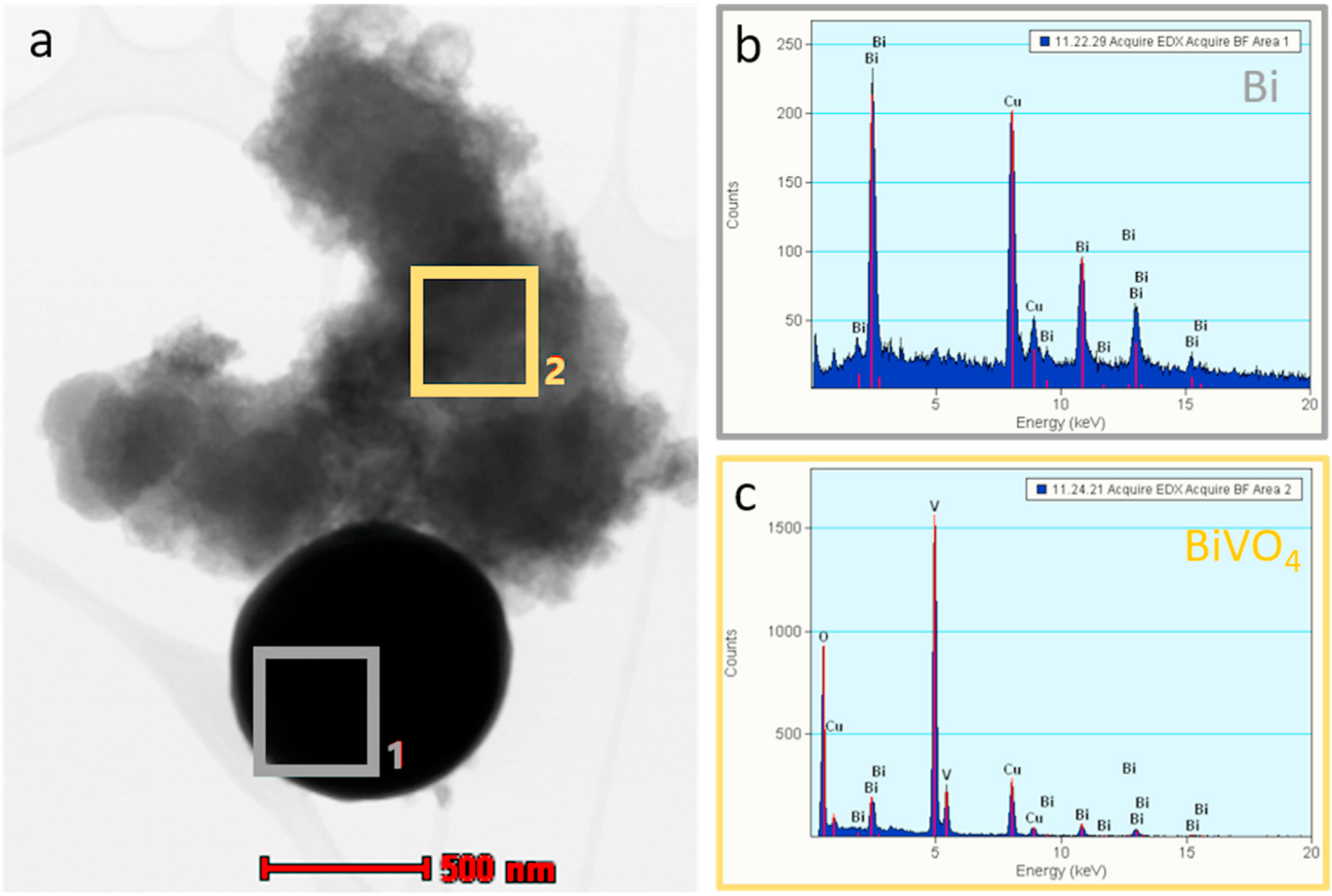


**Fig. 4.** a) TEM image of Bi–$BiVO_4$ highlighting regions 1 and 2, b) EDS from region 1 and c) EDS from region 2 of the Bi–$BiVO_4$ semiconductor. The sample was prepared using microwave synthesis at 240 °C for 5 min without magnetic stirring.

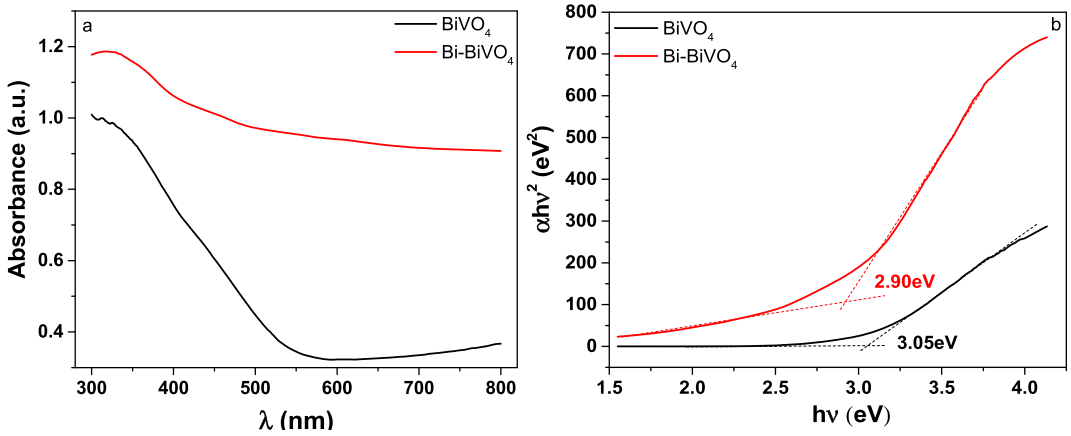


**Fig. 5.** a) DRS analysis in the UV–Vis region for Bi–$BiVO_4$ (red curve) and $BiVO_4$ (black curve) semiconductors prepared using microwave synthesis and b) Tauc plot for determination of the band gap, considering the direct electronic transition. (For interpretation of the references to colour in this figure legend, the reader is referred to the Web version of this article.)

catalyst surface. Dong and coworkers [57] affirm that the incorporation of Bi into other catalysts brings more than one benefit: (i) it improves the light-harvesting ability ranging from UV to near-infrared light, favoring the active production of electrons and holes, (ii) it can induce a built-in electric field that accelerates the separation of photo-excited electrons and holes, and (iii) the Bi nanoparticles could act as electron traps facilitating the separation of electron-hole pairs. Those characteristics proved to be interesting for application in $CO_2$ reduction, considering that they favored the formation of methanol and acetone, something not previously reported in the literature.

Basically, the mechanism of charge transfer of the Bi–$BiVO_4$ catalyst occurs through the photoactivation of the $BiVO_4$ semiconductor by the incidence of light, with energy higher than its

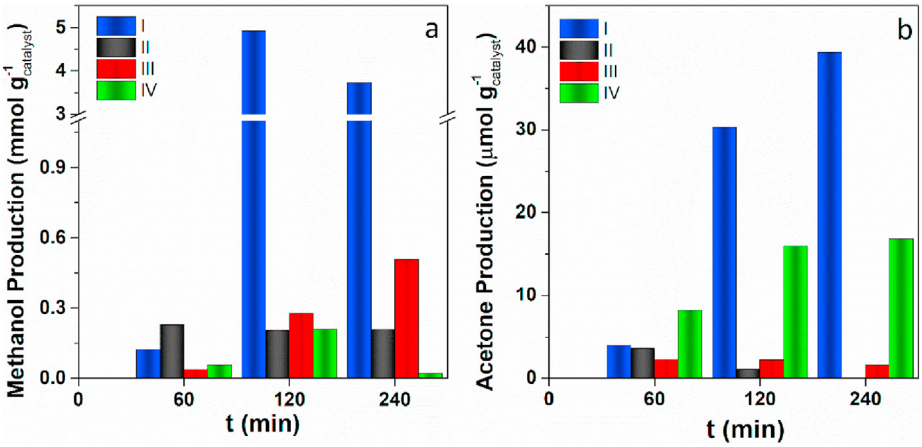


**Fig. 6.** a) Methanol and b) acetone yields from the photoreduction of $CO_2$ using Bi–$BiVO_4$ catalysts obtained by microwave synthesis at 240 °C and (I) 5 min without magnetic stirring, (II) 15 min without magnetic stirring, (III) 5 min under magnetic stirring at 1200 rpm, and (IV) 15 min under magnetic stirring at 1200 rpm.

band gap [58], as well as the photoexcitation of metallic Bi. The absorption of this energy transfers the electrons ($e^-$) from the valence band (VB) to the conduction band (CB). The absence of electrons in the VB generates the holes ($h^+$) and the charges are naturally driven to lower energy regions. Since the $BiVO_4$ CB is at −0.48 eV [5] and the Fermi level of Bi is at −0.17 eV [59], the photoexcited electrons in the $BiVO_4$ surface are injected to the metallic Bi nearby. The photogenerated $h^+$ is responsible for the oxidation of water with the formation of protons ($H^+$), while the photogenerated $e^-$ can reduce the $CO_2$ to $-CO_2^{\bullet}$. After this first step, consecutive reactions with $e^-$ and $H^+$ are responsible for the generation of products via different pathways [60]. Methanol formation requires 6 $e^-$ and 6 $H^+$, while acetone is a highly complex product, requiring 16 $e^-$ and 16 $H^+$ to be formed [61,62]. In this way, metallic Bi functions as a cocatalyst in the $CO_2$ reduction. A summary of the charge transfer mechanism for the Bi–$BiVO_4$ catalyst is presented in Fig. 7. A complete mechanism presenting all steps for the reduction of $CO_2$ by photocatalysis with the formation of methanol and acetone, using $BiVO_4$ as a photocatalyst, was presented in our previous study [5].

Additionally, comparing the results obtained from the best conditions of the present study with other studies reported in the literature about the photocatalytic (PC) reduction of $CO_2$, using powdered photocatalysts under similar experimental conditions, it is easy to observe the improvement of the methanol production by the addition of the Bi cocatalyst, mainly related to the formation of acetone, which was not identified or did not achieve similar values in other studies, as shown in Table 2.

## 4. Conclusion

Here, new Bi–$BiVO_4$ catalysts were prepared using microwave synthesis at 240 °C, employing different reaction times and magnetic stirring regimes. The catalysts were applied in the photosynthetic $CO_2$ reduction in an aqueous medium, using photocatalysis techniques, from which methanol and acetone were produced. Bi–$BiVO_4$ prepared at 240 °C, for 5 min, and without magnetic stirring, produces around 5.0 mmol $L^{-1}$ $g^{-1}_{catalyst}$ of methanol after 240 min of reaction, a threefold improvement compared to previous reports for the pure $BiVO_4$ catalyst. The acetone yield reached 40 μmol $L^{-1}$ $g^{-1}_{catalyst}$ after 240 min for the same catalyst. In this case, metallic Bi works as a cocatalyst improving the activity of $BiVO_4$ for $CO_2$ reduction, enhancing the absorption of visible light by the catalyst, inducing a built-in electric field, and acting as electron traps; moreover, a Schottky barrier is formed, which improves the density of photogenerated electrons

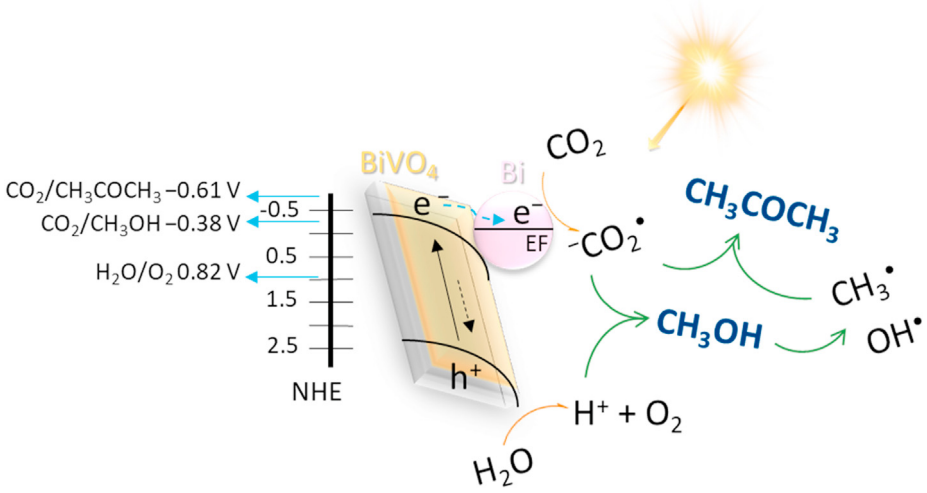


**Fig. 7.** Mechanism of charge transfer from the photoexcited lamellar Bi–$BiVO_4$ semiconductor to $CO_2$ showing the formation of methanol and acetone.

**Table 2**
$CO_2$ reduction by photocatalysis using powdered catalysts and its products reported in the literature.

| Powdered photocatalyst | Experimental Conditions | Concentration of Products | Ref. |
|---|---|---|---|
| Cu(II) nanocluster-grafted $Nb_3O_8^-$ nanosheets | 0.5 mol $L^{-1}$ $KHCO_3$ pH 12, saturated with $CO_2$ (100 mL $min^{-1}$), Hg–Xe lamp (240–300 nm) | 1.4 μmol CO | [2] |
| $Cu_2O$ octahedrons/$WO_3$ nanoflakes | Water vapor, 300 W Xe lamp | 3.84 μmol CO<br>2.22 μmol $CH_4$ | [63] |
| NiFe layered double hydroxides/$Cu_2O$ | Gas-phase reactor, 300 W Xe lamp coupled with 420 nm cut-off filter | 3.33 μmol $g^{-1}$ $CH_4$ | [64] |
| Cu(II)porphyrin | 100 mL $H_2O$ containing 1 mL triethylamine, at 5 °C, 300 W Xe arc lamp | 262.6 ppm $g^{-1}$ $h^{-1}$ $CH_3OH$ | [65] |
| Co(II)porphyrin/Carbon nitride | 1 mL Triethanolamine and 4 mL MeCN, 80 kPa of pure $CO_2$ gas, visible light from 300 W Xe arc lamp | 17 μmol $g^{-1}$ $h^{-1}$ CO | [66] |
| Cr–Ce mixed oxides | Gas-phase reactor, 300 W Xe lamp coupled with 420 nm cut-off filter | 60 μmol $g^{-1}$ $CH_4$<br>15 μmol $g^{-1}$ $CH_3OH$ | [67] |
| Si/Ti | Water saturated with $CO_2$ (50 mL $min^{-1}$), UV lamp 300 W | 4.14 μmol $g^{-1}$ $h^{-1}$ $CH_4$<br>1.45 μmol $g^{-1}$ $h^{-1}$ CO<br>0.03 μmol $g^{-1}$ $h^{-1}$ $CH_3OH$ | [68] |
| *o*-$BiVO_4$ layer | Water with pure $CO_2$ gas (0.5 mL $min^{-1}$), 300 W Xe lamp (100 mW $cm^{-2}$), 0 °C | 398.3 μmol $g^{-1}$ $h^{-1}$ $CH_3OH$ | [33] |
| $BiVO_4$-lamellar | 0.1 mol $L^{-1}$ $NaHCO_3$, 125 W Hg lamp, 5 °C, 240 min | 1.25 mmol $L^{-1}$ $g^{-1}$ $CH_3OH$<br>15 μmol $L^{-1}$ $g^{-1}$ $CH_3COCH_3$ | [5] |
| g-$C_3N_4$/Bi/$BiVO_4$ | Water vapor, $NaHCO_3$ powder and $H_2SO_4$ solution, 300 W Xe lamp ($\lambda \leq 420$ nm) | 1.25 μmol $g^{-1}$ $h^{-1}$ CO<br>0.10 μmol $g^{-1}$ $h^{-1}$ $CH_3OH$<br>0.10 μmol $g^{-1}$ $h^{-1}$ $CH_4$ | [69] |
| Bi–$BiVO_4$ | 0.1 mol $L^{-1}$ $NaHCO_3$, 125 W Hg lamp, 5 °C, 240 min | 5.0 mmol $L^{-1}$ $g^{-1}$ $CH_3OH$<br>40 μmol $L^{-1}$ $g^{-1}$ $CH_3COCH_3$ | This study |

and holes in the surface of the catalyst. The mechanism of charge transfer between $BiVO_4$ and the metallic Bi is also influenced by the size of the microsphere crystallites, since smaller crystallite sizes produce better methanol yields. The catalyst architecture improves the results of $CO_2$ reduction due to the increase of the surface area, minimization of the charge recombination, and improvement of the velocity of charge carrier transportation, making Bi–$BiVO_4$ an attractive semiconductor for the photocatalytic reduction of $CO_2$.

## CRediT authorship contribution statement

**Juliana F. de Brito:** Investigation, Methodology, Data curation, Writing - original draft, Writing - review & editing. **Patricia G. Corradini:** Investigation, Methodology, Data curation, Writing - original draft, Writing - review & editing. **Maria Valnice B. Zanoni:** Methodology, Writing - review & editing. **Frank Marken:** Visualization, Writing - review & editing. **Lucia H. Mascaro:** Visualization, Supervision, Writing - review & editing, Resources.

## Declaration of competing interest

The authors declare that they have no known competing financial interests or personal relationships that could have appeared to influence the work reported in this paper.

## Acknowledgment

The authors thank the Laboratory of Structural Characterization, LCE/DEMa/UFSCar, for the general facilities. The authors are grateful to the following Brazilian research funding agencies for the financial support provided during the course of this research: São Paulo Research Foundation, FAPESP [grant #2018/16401-8, #2018/02950-0, #2013/07296-2, #2014/50249-8, #2017/1198-5], Coordenação de Aperfeiçoamento de Pessoal de Nível Superior – Brasil, CAPES [001], Conselho Nacional de Pesquisa e Desenvolvimento, CNPq, and INCT-DATREM [#465571/2014-0].

## References

[1] T. Takayama, K. Sato, T. Fujimura, Y. Kojima, A. Iwase, A. Kudo, Photocatalytic CO2 reduction using water as an electron donor by a powdered: Z -scheme system consisting of metal sulfide and an RGO-TiO2 composite, Faraday Discuss 198 (2017) 397–407, https://doi.org/10.1039/c6fd00215c.
[2] G. Yin, M. Nishikawa, Y. Nosaka, N. Srinivasan, D. Atarashi, E. Sakai, M. Miyauchi, Photocatalytic carbon dioxide reduction by copper oxide nanocluster-grafted niobate nanosheets, ACS Nano 9 (2015) 2111–2119, https://doi.org/10.1021/nn507429e.
[3] J. Fu, K. Jiang, X. Qiu, J. Yu, M. Liu, Product selectivity of photocatalytic CO2 reduction reactions, Mater. Today 32 (2020) 222–243, https://doi.org/10.1016/j.mattod.2019.06.009.
[4] L. Shan, C. Lu, L. Dong, J. Suriyaprakash, Efficient facet regulation of BiVO4 and its photocatalytic motivation, J. Alloys Compd. 804 (2019) 385–391, https://doi.org/10.1016/j.jallcom.2019.07.051.
[5] P.G. Corradini, J.F. De Brito, M.V. Boldrin Zanoni, L.H. Mascaro, Artificial photosynthesis for alcohol and 3-C compound formation using BiVO4-lamelar catalyst, J. CO2 Util. 36 (2020) 187–195, https://doi.org/10.1016/j.jcou.2019.10.020.
[6] X. Li, L. Xu, X. Li, M. Hu, R. Huang, C. Huang, Oxidant peroxo-synthesized monoclinic BiVO4: insights into the crystal structure deformation and the thermochromic properties, J. Alloys Compd. 787 (2019) 666–671, https://doi.org/10.1016/j.jallcom.2019.02.136.
[7] B.J. Yu, A. Kudo, Effects of structural variation on the photocatalytic performance of hydrothermally synthesized BiVO4 **, Adv. Funct. Mater. Mater. 16 (2006) 2163–2169, https://doi.org/10.1002/adfm.200500799.
[8] L.H. Mascaro, A. Pockett, J.M. Mitchels, L.M. Peter, P.J. Cameron, V. Celorrio, D.J. Fermin, J.S. Sagu, K.G.U. Wijayantha, G. Kociok-Köhn, F. Marken, One-step preparation of the BiVO4 film photoelectrode, J. Solid State Electrochem. 19 (2014) 31–35, https://doi.org/10.1007/s10008-014-2495-y.
[9] D. Wang, H. Jiang, X. Zong, Q. Xu, Y. Ma, G. Li, C. Li, Crystal facet dependence of Water oxidation on BiVO4 sheets under visible light irradiation, Chem. Eur J. 17 (2011) 1275–1282, https://doi.org/10.1002/chem.201001636.
[10] D. Ke, T. Peng, L. Ma, P. Cai, K. Dai, Effects of hydrothermal temperature on the microstructures of BiVO 4 and its photocatalytic O2 evolution activity under visible light, Inorg. Chem. 48 (2009) 4685–4691, https://doi.org/10.1021/ic900064m.
[11] D. Coelho, J.P.R.S. Gaudêncio, S.A. Carminati, W.P. Ribeiro, A.F. Nogueira, L.H. Mascaro, Bi electrodeposition on WO3 photoanode to improve the photoactivity of the WO3/BiVO4 heterostructure to water splitting, Chem. Eng. J. 339 (2020) 125836, https://doi.org/10.1016/j.cej.2020.125836.
[12] N.I.M. Abdallah, Y. Li, X.T. Wang, X. Li, C.W. Wang, Design and fabrication of

Ni(OH)2/BiVO4 heterostructured nano-photocatalyst for high-efficient removal of organic dyes, J. Alloys Compd. 831 (2020) 154828, https://doi.org/10.1016/j.jallcom.2020.154828.
[13] W. Fang, R. Tao, Z. Jin, Z. Sun, F. Li, L. Xu, Sandwich-type cobalt-polyoxometalate as an effective hole extraction layer for enhancing BiVO4-based photoelectrochemical oxidation, J. Alloys Compd. 797 (2019) 140–147, https://doi.org/10.1016/j.jallcom.2019.05.063.
[14] S. Gao, B. Gu, X. Jiao, Y. Sun, X. Zu, F. Yang, W. Zhu, C. Wang, Z. Feng, B. Ye, Y. Xie, Highly efficient and exceptionally durable CO2 photoreduction to methanol over freestanding defective single-unit-cell bismuth vanadate layers, J. Am. Chem. Soc. 139 (2017) 3438–3445, https://doi.org/10.1021/jacs.6b11263.
[15] Y. Liu, B. Huang, Y. Dai, X. Zhang, X. Qin, M. Jiang, M.H. Whangbo, Selective ethanol formation from photocatalytic reduction of carbon dioxide in water with BiVO4 photocatalyst, Catal. Commun. 11 (2009) 210–213, https://doi.org/10.1016/j.catcom.2009.10.010.
[16] J.M. Sommers, N.P. Alderman, C.J. Viasus, S. Gambarotta, Revisiting the behaviour of BiVO4 as a carbon dioxide reduction photo-catalyst, Dalton Trans. 46 (2017) 6404–6408, https://doi.org/10.1039/c7dt00414a.
[17] X. Chen, L. Li, T. Yi, W. Zhang, X. Zhang, L. Wang, Microwave assisted synthesis of sheet-like Cu/BiVO4 and its activities of various photocatalytic conditions, J. Solid State Chem. 229 (2015) 141–149, https://doi.org/10.1016/j.jssc.2015.05.026.
[18] V.I. Merupo, S. Velumani, G. Oza, M. Makowska-Janusik, A. Kassiba, Structural, electronic and optical features of molybdenum-doped bismuth vanadium oxide, Mater. Sci. Semicond. Process. 31 (2015) 618–623, https://doi.org/10.1016/j.mssp.2014.12.057.
[19] M. Long, W. Cai, J. Cai, B. Zhou, X. Chai, Y. Wu, Efficient photocatalytic degradation of phenol over Co3O4/BiVO4 composite under visible light irradiation, J. Phys. Chem. B 110 (2006) 20211–20216.
[20] H. Maimaitizi, A. Abulizi, K. Kadeer, D. Talifu, Y. Tursun, In situ synthesis of Pt and N co-doped hollow hierarchical BiOCl microsphere as an efficient photocatalyst for organic pollutant degradation and photocatalytic CO2 reduction, Appl. Surf. Sci. 502 (2020) 144083, https://doi.org/10.1016/j.apsusc.2019.144083.
[21] X. Zhao, Z. Duan, L. Chen, Bi-quantum-dot-decorated Bi4V2O11 hollow nanocakes: synthesis, characterization, and application as photocatalysts for CO2 reduction, Ind. Eng. Chem. Res. 58 (2019) 10402–10409, https://doi.org/10.1021/acs.iecr.9b01737.
[22] A. Walsh, Y. Yan, M.N. Huda, M.M. Al-jassim, S. Wei, Band edge electronic structure of BiVO4 : elucidating the role of the Bi s and V d orbitals, Chem. Mater. 21 (2009) 547–551.
[23] S. Li, J. Chen, S. Hu, W. Jiang, Y. Liua, J. Liu, A novel 3D Z-scheme heterojunction photocatalyst: Ag6Si2O7 anchored on flower-like Bi2WO6 and its excellent photocatalytic performance for the degradation of toxic pharmaceutical antibiotics †, Inorg. Chem. Front. 7 (2020) 529–541, https://doi.org/10.1039/c9qi01201j.
[24] S. Li, J. Chen, W. Jiang, Y. Liu, Y. Ge, J. Liu, Facile construction of flower-like bismuth oxybromide/bismuth oxide formate p-n heterojunctions with significantly enhanced photocatalytic performance under visible light, J. Colloid Interface Sci. 548 (2019) 12–19, https://doi.org/10.1016/j.jcis.2019.04.024.
[25] S. Li, S. Hu, W. Jiang, J. Zhang, K. Xu, Z. Wang, In situ construction of WO3 nanoparticles decorated Bi2MoO6 microspheres for boosting photocatalytic degradation of refractory pollutants, J. Colloid Interface Sci. 556 (2019) 335–344, https://doi.org/10.1016/j.jcis.2019.08.077.
[26] S. Li, X. Shen, J. Liu, L. Zhang, Synthesis of Ta3N5/Bi2MoO6 core-shell fiber-shaped heterojunctions as efficient and easily recyclable photocatalysts, Environ. Sci. Nano. 4 (2017) 1155–1167, https://doi.org/10.1039/C6EN00706F.
[27] A. Aranda-aguirre, J. Ojeda, J.F. de Brito, S. Garcia-segura, M.V.B. Zanoni, H. Alarcon, Photoelectrodes of Cu2O with interfacial structure of topological insulator Bi2Se3 contributes to selective photoelectrocatalytic reduction of CO2 towards methanol, J. CO2 Util. 39 (2020) 101154, https://doi.org/10.1016/j.jcou.2020.101154.
[28] J.F. de Brito, K. Irikura, C.M. Terzi, S. Nakagaki, M.V.B. Zanoni, The great performance of TiO2 nanotubes electrodes modified by copper(II)porphyrin in the reduction of carbon dioxide to alcohol, J. CO2 Util. 41 (2020) 101261, https://doi.org/10.1016/j.jcou.2020.101261.
[29] J. de Almeida, M.S. Pacheco, J.F. de Brito, C. de Arruda Rodrigues, Contribution of CuxO distribution, shape and ratio on TiO2 nanotubes to improve methanol production from CO2 photo electroreduction, J. Solid State Electrochem. (2020), https://doi.org/10.1007/s10008-020-04739-3.
[30] C. Kim, K.M. Cho, A. Al-Saggaf, I. Gereige, H.T. Jung, Z-scheme photocatalytic CO2 conversion on three-dimensional BiVO4/carbon-coated Cu2O nanowire arrays under visible light, ACS Catal. 8 (2018) 4170–4177, https://doi.org/10.1021/acscatal.8b00003.
[31] M.F. Gromboni, D. Coelho, L.H. Mascaro, A. Pockett, F. Marken, Enhancing activity in a nanostructured BiVO4 photoanode with a coating of microporous Al2O3, Appl. Catal. B Environ. 200 (2017) 133–140, https://doi.org/10.1016/j.apcatb.2016.06.059.
[32] L. Wang, S. Zhang, S. Wu, Y. Long, L. Li, Z. Zheng, Y. Hei, L. Zhou, L. Luo, F. Jiang, Controlling wettability of AgI/BiVO4 composite photocatalyst and its effect on photocatalytic performance, J. Alloys Compd. 835 (2020) 155367, https://doi.org/10.1016/j.jallcom.2020.155367.
[33] S. Gao, B. Gu, X. Jiao, Y. Sun, X. Zu, F. Yang, W. Zhu, C. Wang, Z. Feng, B. Ye, Y. Xie, Highly efficient and exceptionally durable CO2 photoreduction to methanol over freestanding defective single-unit-cell bismuth vanadate layers, J. Am. Chem. Soc. 139 (2017) 3438–3445, https://doi.org/10.1021/jacs.6b11263.
[34] A. Dolgonos, T.O. Mason, R. Kenneth, Direct optical band gap measurement in polycrystalline semiconductors: a critical look at the Tauc method, J. Solid State Chem. 240 (2016) 43–48, https://doi.org/10.1016/j.jssc.2016.05.010.
[35] O. Hunderi, Optical properties of crystalline and amorphous bismuth films, J. Phys. F Met. Phys. 5 (1975) 2214–2225, https://doi.org/10.1088/0305-4608/5/11/034.
[36] Z. Wang, C. Jiang, R. Huang, H. Peng, X. Tang, The investigation of optical and photocatalytic properties of bismuth nanospheres prepared by a facile thermolysis method the investigation of optical and photocatalytic properties of bismuth nanospheres prepared by a facile thermolysis method key laborat, J. Phys. Chem. C 118 (2014) 1155–1160.
[37] M. Ahila, M. Malligavathy, E. Subramanian, D. Pathinettam Padiyan, Effect of anodization time on the growth of twinned pyramid crystals of bismite from polyhedral bismuth particle by facile electrolysis-based oxidation, Part. Sci. Technol. 36 (2018) 655–659, https://doi.org/10.1080/02726351.2017.1287793.
[38] G. Zhao, W. Liu, J. Li, Q. Lv, W. Li, L. Liang, Facile synthesis of hierarchically structured BiVO4 oriented along (010) facets with different morphologies and their photocatalytic properties, Appl. Surf. Sci. 390 (2016) 531–539, https://doi.org/10.1016/j.apsusc.2016.08.126.
[39] M. Wu, Q. Jing, X. Feng, L. Chen, BiVO 4 microstructures with various morphologies: synthesis and characterization, Appl. Surf. Sci. 427 (2018) 525–532, https://doi.org/10.1016/j.apsusc.2017.07.299.
[40] U.M. García-Pérez, A. Martínez-De La Cruz, S. Sepúlveda-Guzmán, J. Peral, Low-temperature synthesis of BiVO4 powders by Pluronic-assisted hydrothermal method: effect of the surfactant and temperature on the morphology and structural control, Ceram. Int. 40 (2014) 4631–4638, https://doi.org/10.1016/j.ceramint.2013.09.002.
[41] J. Madhavi, Comparison of average crystallite size by X-ray peak broadening and Williamson–Hall and size–strain plots for VO2+ doped ZnS/CdS composite nanopowder, SN Appl. Sci. 1 (2019) 1–12, https://doi.org/10.1007/s42452-019-1291-9.
[42] B. Lei, L. Zeng, P. Zhang, Z. Sun, W. Sun, X. Zhang, Hydrothermal synthesis and photocatalytic properties of visible-light induced BiVO4 with different morphologies, Adv. Powder Technol. 25 (2014) 946–951, https://doi.org/10.1016/j.apt.2014.01.014.
[43] B. Wunderlich, Chapter V - the nucleation step. Macromol. Phys. Cryst. Nucleation, Growth, Annealing, Elsevier Inc., 1976, pp. 1–114, https://doi.org/10.1016/B978-0-12-765602-1.50007-0.
[44] Bernhard Wunderlich, Chapter VI - the growth of crystals. Macromol. Phys. Cryst. Nucleation, Growth, Annealing, Elsevier Inc., 1976, pp. 1–114, https://doi.org/10.1016/B978-0-12-765602-1.50008-2.
[45] J.F. Brito, A.A. Silva, A.J. Cavalheiro, M.V.B. Zanoni, Evaluation of the parameters affecting the photoelectrocatalytic reduction of CO2 to CH3OH at Cu/Cu2O electrode, Int. J. Electrochem. Sci. 9 (2014) 5961–5973.
[46] A. Dey, D. Maiti, G.K. Lahiri, Photoelectrocatalytic reduction of CO2 into C1 products by using modified-semiconductor-based catalyst systems, Asian J. Org. Chem. 6 (2017) 1519–1530, https://doi.org/10.1002/ajoc.201700351.
[47] W. Li, Electrocatalytic reduction of CO2 to small organic molecule fuels on metal catalysts wenzhen, Adv CO2 Convers. Util., ACS Symp. Ser. 1056 (2010) 55–76, https://doi.org/10.1021/bk-2010-1056.ch005.
[48] C. Costentin, M. Robert, J. Save, Catalysis of the electrochemical reduction of carbon dioxide†, Chem. Soc. Rev. 42 (2013) 2423–2436, https://doi.org/10.1039/c2cs35360a.
[49] X. Chang, T. Wang, J. Gong, CO2 photo-reduction: insights into CO2 activation and reaction on surfaces of photocatalysts, Energy Environ. Sci. 9 (2016) 2177–2196, https://doi.org/10.1039/c6ee00383d.
[50] J. Yuan, X. Wang, C. Gu, J. Sun, W. Ding, J. Wei, X. Zuo, C. Hao, Photoelectrocatalytic reduction of carbon dioxide to methanol at cuprous oxide foam cathode, RSC Adv. 7 (2017) 24933–24939, https://doi.org/10.1039/C7RA03347H.
[51] W. Wei, Z. Yang, W. Song, F. Hu, B. Luan, P. Li, H. Yin, Different CdSeTe structure determined photoelectrocatalytic reduction performance for carbon dioxide, J. Colloid Interface Sci. 496 (2017) 327–333, https://doi.org/10.1016/j.jcis.2016.11.054.
[52] A. Varga, G.F. Samu, C. Janáky, Rapid synthesis of interconnected CuCrO2 nanostructures: a promising electrode material material for photoelectrochemical fuel generation, Electrochim. Acta 272 (2018) 22–32, https://doi.org/10.1016/j.electacta.2018.03.185.
[53] T.T. Guaraldo, J.F. de Brito, D. Wood, M.V.B. Zanoni, A new Si/TiO2/Pt p-n junction semiconductor to demonstrate photoelectrochemical CO 2 conversion, Electrochim. Acta 185 (2015) 117–124, https://doi.org/10.1016/j.electacta.2015.10.077.
[54] S.Y. Noh, K. Sun, C. Choi, M. Niu, M. Yang, K. Xu, S. Jin, D. Wang, Branched TiO2/Si nanostructures for enhanced photoelectrochemical water splitting, Nanomater. Energy 2 (2013) 351–360, https://doi.org/10.1016/j.nanoen.2012.10.010.
[55] J. Zhao, Y. Li, Y. Zhu, Y. Wang, C. Wang, Enhanced CO2 photoreduction activity of black TiO2–coated Cu nanoparticles under visible light irradiation: role of metallic Cu, Appl. Catal. Gen. 510 (2016) 34–41.
[56] L.M. Castillo, L.M. Peter, INTERNAL PHOTOEMISSION AT THE Bi/ANODIC Bi203

INTERFACE, J. Electroanal. Chem. 146 (1983) 377–384.
[57] F. Dong, Z. Zhao, Y. Sun, Y. Zhang, S. Yan, Z. Wu, An advanced semimetal-organic Bi spheres-g-C3N4 nanohybrid with SPR-enhanced visible-light photocatalytic performance for NO purification, Environ. Sci. Technol. 49 (2015) 12432–12440, https://doi.org/10.1021/acs.est.5b03758.
[58] J.F. de Brito, F.F. Hudari, M.V.B. Zanoni, Photoelectrocatalytic performance of nanostructured p-n junction NtTiO 2/NsCuO electrode in the selective conversion of CO 2 to methanol at low bias potentials, J. CO2 Util. 24 (2018) 81–88, https://doi.org/10.1016/j.jcou.2017.12.008.
[59] F. Dong, Q. Li, Y. Sun, W.K. Ho, Noble metal-like behavior of plasmonic Bi particles as a cocatalyst deposited on (BiO)2CO3 microspheres for efficient visible light photocatalysis, ACS Catal. 4 (2014) 4341–4350, https://doi.org/10.1021/cs501038q.
[60] J.F. de Brito, M.V.B. Zanoni, On the application of Ti/TiO2/CuO n-p junction semiconductor : a case study of electrolyte, temperature and potential influence on CO2 reduction, Chem. Eng. J. 318 (2017) 264–271, https://doi.org/10.1016/j.cej.2016.08.033.
[61] E. Kecsenovity, B. Endrődi, P.S. Tóth, Y. Zou, R.A.W. Dryfe, K. Rajeshwar, C. Janáky, Enhanced photoelectrochemical performance of cuprous oxide/graphene nanohybrids, J. Am. Chem. Soc. 139 (2017) 6682–6692, https://doi.org/10.1021/jacs.7b01820.
[62] J.F. Brito, A.R. Araújo, K. Rajeshwar, M.V.B. Zanoni, Photoelectrochemical reduction of CO2 on Cu/Cu2 O films: product distribution and pH effects, Chem. Eng. J. 264 (2015) 302–309, https://doi.org/10.1016/j.cej.2014.11.081.
[63] W. Shi, X. Guo, J. Wang, Y. Li, L. Liu, Y. Hou, Y. Li, H. Lou, Enhanced photocatalytic 3D/2D architecture for CO2 reduction over cuprous oxide octahedrons supported on hexagonal phase tungsten oxide nanoflakes, J. Alloys Compd. 830 (2020) 2–8, https://doi.org/10.1016/j.jallcom.2020.154683.
[64] Y. Wu, Y. Gong, J. Liu, T. Chen, Q. Liu, Y. Zhu, L. Niu, C. Li, X. Liu, C.Q. Sun, S. Xu, Constructing NiFe-LDH wrapped Cu2O nanocube heterostructure photocatalysts for enhanced photocatalytic dye degradation and CO2 reduction via Z-scheme mechanism, J. Alloys Compd. 831 (2020) 154723, https://doi.org/10.1016/j.jallcom.2020.154723.
[65] Y. Liu, Y. Yang, Q. Sun, Z. Wang, B. Huang, Y. Dai, X. Qin, Chemical adsorption enhanced CO2 capture and photoreduction over a copper porphyrin based metal organic framework, ACS Appl. Mater. Interfaces 5 (2013) 7654–7658.
[66] G. Zhao, H. Pang, G. Liu, P. Li, H. Liu, H. Zhang, L. Shi, J. Ye, Co-porphyrin/Carbon nitride hybrids for improved photocatalytic CO2 reduction under visible light, Appl. Catal. B Environ. (2016), https://doi.org/10.1016/j.apcatb.2016.06.074.
[67] Y. Zhao, W. Cai, M. Chen, Y. Bu, Turning the activity of Cr e Ce mixed oxide towards thermocatalytic NO oxidation and photocatalytic CO2 reduction via the formation of yolk shell structure hollow microspheres, J. Alloys Compd. 829 (2020) 154508, https://doi.org/10.1016/j.jallcom.2020.154508.
[68] P. Akhter, M. Hussain, G. Saracco, N. Russo, New nanostructured silica incorporated with isolated Ti material for the photocatalytic conversion of CO 2 to fuels, Nanoscale Res. Lett. 9 (2014) 1–8.
[69] Q. Xie, W. He, S. Liu, C. Li, J. Zhang, P.K. Wong, Bifunctional S-scheme g-C3N4/Bi/BiVO4 hybrid photocatalysts toward artificial carbon cycling, Chin. J. Catal. 41 (2020) 140–153, https://doi.org/10.1016/S1872-2067(19)63481-9.